Transactions of the Materials Research Society of Japan 32[1] 19-22 (2007)

Polarization Dependence for Electronic Structure of $Bi_4Ti_3O_{12}$ Single Crystal Probed by Soft-X-Ray Raman Scattering

Tohru Higuchi, Takeshi Hattori and Takeyo Tsukamoto
Department of Applied Physics, Tokyo University of Science, 1-3 Kagurazaka, Shinjuku, Tokyo 162-8601, Japan
Fax: 81-3-3260-4772, e-mail: higuchi@rs.kagu.tus.ac.jp

The polarization dependence for the electronic structure of $Bi_4Ti_3O_{12}$ (BIT) single crystal has been studied by soft-X-ray emission spectroscopy (SXES) and X-ray absorption spectroscopy (XAS). The valence band and conduction band are mainly composed of O 2*p* state and Ti 3*d* state, respectively. The SXES spectra measured at the Ti 2*p* absorption edge region exhibit three structures, which correspond to elastic scattering, fluorescence and soft-X-ray Raman scattering. The Raman scattering corresponds to the charge-transfer (CT) energy, which corresponds to the transition from O 2*p* state to unoccupied Ti 3*d* state. The CT energy in the *a-c* plane is different from that in the *a-b* plane. The difference of CT energy originates to the lattice constant and hybridization effect in BIT single crystal.

Key words: $Bi_4Ti_3O_{12}$ (BIT), soft-X-ray Raman scattering, electronic structure, charge transfer (CT), polarization

1. INTRODUCTION

Ferroelectric $Bi_4Ti_3O_{12}$ (BIT) consists of the layer structure of $Bi_2O_2^{2+}$ and a pseudoperovskite along the c-axis. The BIT exhibits ferroelectricity along both the *a*- and *c*-axes [1-3]. It shows coercive fields (E_c) of 3.5 kV/cm and 50 kV/cm, spontaneous polarization (P_s) values of 4 μC/cm^2 and 50 μC/cm^2, and dielectric constants (ε) of 130 and 160 along the *c*- and *a*-axis, respectively. Furthermore, the BIT exhibits high Curie temperature and large electro-optic coefficient [4-6]. The control of polarization state is the underlying basis of these functional devices, and domain switching by applying electric field can only be achieved with a high insulative property. Therefore, the structural and electrical properties have been extensively studied in the single crystal and ceramic forms [7-16].

In this study, the polarization dependence for the electronic structure of BIT single crystal has been investigated by soft-X-ray emission spectroscopy (SXES) and X-ray absorption spectroscopy (XAS). The SXES and XAS techniques can investigate the electronic structure of the bulk state compared with photoemission spectra, because the mean free path of a soft-X-ray is very long compared with that of an electron. The SXES and XAS have a clear selection rule regarding the angular momentum due to a dipole transition, as it occurs mainly within the same atomic species. Thus, SXES and XAS spectra reflect the partial density of states (PDOS) of occupied and unoccupied states, respectively. In order to probe the crystal anisotropy for electronic structure of BIT single crystal, we measured the polarization dependence of SXES spectra.

2. EXPERIMENTAL

BIT single crystal was grown by the flux method. The XRD pattern of the single crystal exhibited the BIT single phase. Then, the P_r, E_c and ε were 4.10 μC/cm^2, 5.1 kV/cm and 140, respectively.

Figure 1 shows a schematic diagram of the SXES experimental system [17]. The incident angle of the soft-X- ray was about 70 °. The SXES spectra were measured at depolarized and polarized configuration. When the SXES spectra were measured at depolarized configuration in Fig. 1(a), the polarization vector of the emitted photon rotates by 90 ° from the polarization vector of the incident photon. In the case of polarized configuration in Fig.1(b), the polarization vector of the emitted photon contains the same polarization vector as that of the incident photon. Thus, the SXES spectra at the polarized and depolarized configurations reflect the electronic structures within the *a-b* plane and *a-c* plane, respectively.

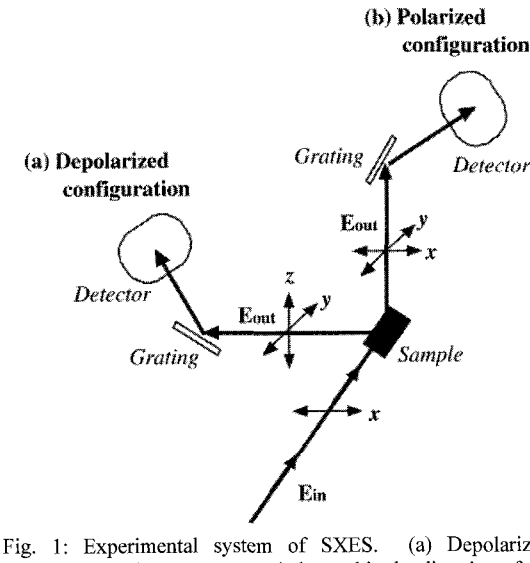

Fig. 1: Experimental system of SXES. (a) Depolarized configuration; the spectrometer is located in the direction of the polarization vector of the incident photon. (b) Polarized configuration; the spectrometer is located normal to the wave vector and the polarization vector of the incident photon.

SXES spectra were measured using a soft-X-ray spectrometer installed at the undulator beamline BL-2C (in Photon Factory) at the High Energy Accelerator Organization. Synchrotron radiation was monochromatized using a varied-line spacing plain grating whose average groove density was 1000 lines/mm. The SXES spectrometer is Rowland Mount type with a laminar grating whose radius and groove density are 5 m and 1200 lines/mm. The total energy resolution was about 0.4 eV at $h\nu$=450 eV with a 20 μm incident slit width of the spectrometer.

3. RESULTS AND DISCUSSION

Figure 2 shows the occupied valence band by O 1*s*, Ti 2*p* SXES and the unoccupied conduction band by O 1*s* XAS of the BIT single crystal. The O 1*s* and Ti 2*p* SXES spectra measured at $h\nu$=550 eV and 480 eV reflect the partial density of state (PDOS) of the O 2*p* state and Ti 3*d* state in the valence band. One can find that the O 2*p* state overlaps with the Ti 3*d* state. This result indicates that the O 2*p* state hybridizes with the Ti 3*d* state in the valence band. Thus, it is clear that feature A corresponds to the nonbonding state and feature B corresponds to the bonding state that is well mixed with the Ti 3*d* state.

From the dipole selection rule, it is understood that the O 1*s* XAS spectra of the Ti compound correspond to transitions from O 1*s* to O 2*p* character hybridized into the unoccupied Ti 3*d* states. Generally, the O 1*s* spectra of Ti oxides shift to a lower energy by about 0.5 eV due to core hole potential. Thus, the bottom axis of the O 1*s* XAS spectrum is calibrated by considering the core hole potential effect. The lower-energy peak is attributed to the O 2*p* state, while the higher-energy peak is attributed to the O 2*p* state. These states are hybridized with Ti 3*d* (t_{2g}) and Ti 3*d* (e_g) states, respectively. The energy separation between the top of the valence band and the bottom of the conduction band reflects the band gap (E_g).

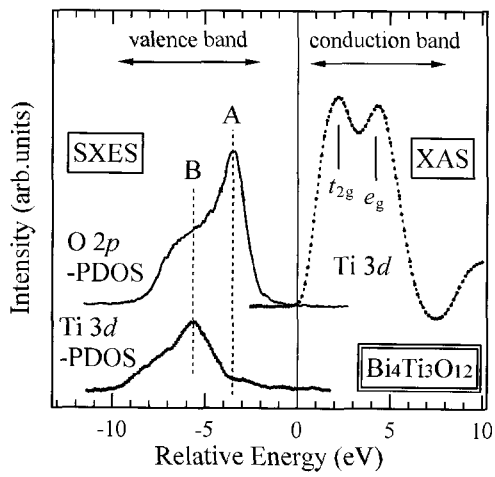

Fig. 2: O 1*s*, Ti 2*p* SXES and O 1*s* XAS spectra of BIT single crystal. The SXES and XAS spectra reflect the band structures of valence band and conduction band, respectively. The peaks A and B indicate the nonbonding state and bonding state, respectively.

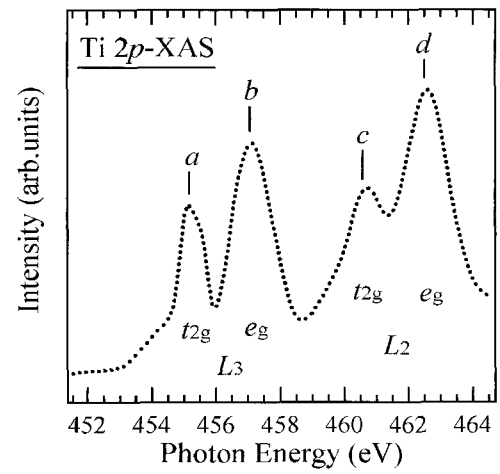

Fig. 3: Ti 2*p* XAS spectrum in the *a*-*b* plane of BIT single crystal.

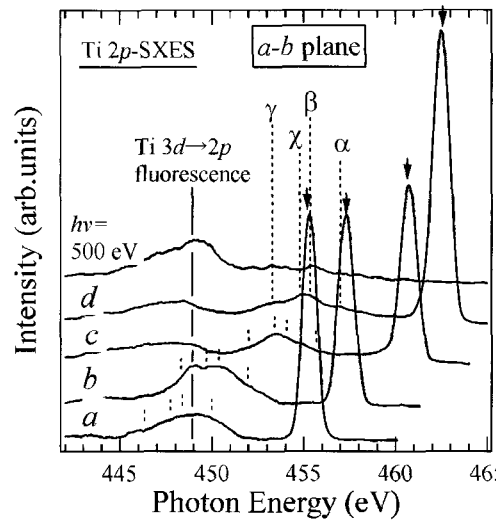

Fig. 4: Ti 2*p* SXES spectra in the *a*-*b* plane excited at various photon energies indicated in Fig. 3. An arrow shows the energy position of the excitation photon energy (elastic scattering). The vertical lines show the energy position of Ti 3d → 2p fluorescence. Four vertical dashed lines (α, β, χ, and γ) are soft-X-ray Raman scattering (inelastic scattering).

Figure 3 shows the Ti 2*p* XAS spectrum of the BIT single crystal. The spectrum is derived from two parts of L_3 ($2p_{3/2}$) and L_2 ($2p_{1/2}$). Furthermore, they are split into t_{2g} and e_g states due to the octahedral ligand field [10,12]. The vertical bars, which are labeled from *a* to *d*, indicate the selected photon energies for resonant SXES measurements.

Figure 4 shows the Ti 2*p* SXES spectra of the BIT single crystal. The Ti 2*p* emission reflects the Ti 3*d* PDOS. The arrow shown in each spectrum indicates the excitation photon energy. The peak beneath the arrow is attributed to the elastic scattering of the excitation photon. The elastic peak is enhanced at the excitation energy corresponding to the t_{2g} absorption peak of L_3. On the other hand, the SXES spectrum excited at $h\nu$=500 eV is an off-resonance spectrum attributed to the normal Ti 3*d* → 2*p* fluorescence

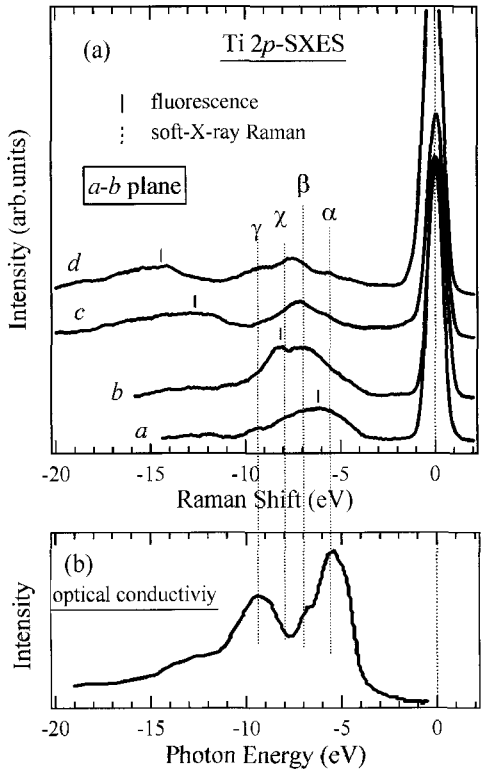

Fig. 5: (a) Ti $3d \rightarrow 2p$ SXES spectra in the *a-b* plane presented as the relative emission energy (Raman shift) to the elastic scattering. The vertical lines are the Ti $3d \rightarrow 2p$ fluorescence. Four vertical dashed lines (α, β, χ, and γ) are soft-X-ray Raman scattering. (b) Optical conductivity spectrum, which corresponds to the transition from O $2p$ to Ti $3d$ states.

spectrum. A vertical line shows the position of the fluorescence band for each SXES spectrum.

Four features shown with vertical bars α, β, χ, and γ represent the energy positions that have energy separation of 5.5, 7.0, 8.0, and 9.2 eV, respectively, from the excitation energy. They shift as the excitation energy is varied. These features are attributed to the soft-X-ray Raman scattering, that is, inelastic scattering. The inelastic scattering that is excited in the L3 absorption spectral region overlaps with the Ti $3d \rightarrow 2p$ fluorescence.

Figure 5 shows the SXES spectra, where the abscissa is the Raman shift (or energy loss) from the elastic scattering. The elastic scattering peak is located at 0 eV. The Ti $3d \rightarrow 2p$ fluorescence peak shifts to a higher energy as the excitation energy increases. In $FeTiO_3$ [18], it is reported that the structures appearing in the energy region between 10 and 4 eV can be attributed to the transition to nonbonding $3d^1\underline{L}$ states and the split-off antibonding satellite is located at 14.5 eV. However, such a satellite is not observed in the SXES spectra.

It is known that the elementary excitation of the Raman scattering is the valence band transition. Thus, the Raman scattering can be compared with the optical conductivity spectrum. The optical conductivity spectrum (Fig. 5(b)) at room temperature is shown under the SXES spectra described by the relative energy Raman Shift. Two prominent peaks are observed at

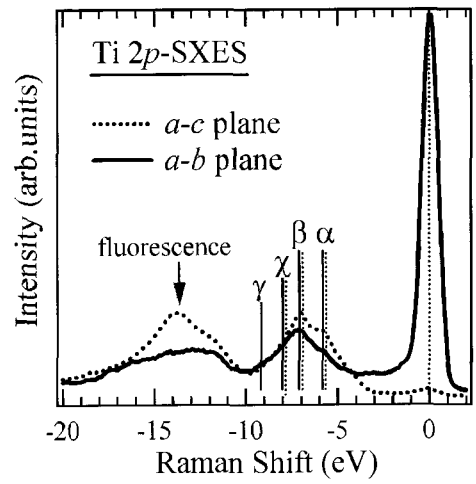

Fig. 6: Ti $3d \rightarrow 2p$ SXES spectra in the *a-c* plane (dashed line) and *a-b* plane (solid line) measured at L_2 (t_{2g}) of Fig. 2. The bottom axis is presented as Raman shift.

~5.5 eV and a weak peak at ~9.2 eV. Four soft-X-ray Raman scattering peaks are in good agreement with the optical conductivity spectrum, as shown in vertical dashed lines (α, β, χ, and γ). These agreements indicate that the soft-X-ray Raman scattering which is attributed to a charge-transfer transition from occupied O $2p$ states to unoccupied Ti $3d$ states [19-24]. Thus, the α peak corresponds to the transition from nonbonding band to t_{2g} subband of Ti $3d$, and the β peak corresponds to the transition from bonding band to t_{2g} subband of Ti $3d$. The χ peak corresponds to the transition from nonbonding band to e_g subband of Ti $3d$, and the γ peak corresponds to the transition from bonding band to e_g subband of Ti $3d$. Furthermore, these energies of soft-X-ray Raman scattering peaks are in agreement with the energy separations of O $2p$ and unoccupied Ti $3d$ state, as shown in Fig. 2.

Figure 6 shows the SXES spectra in the *a-b* plane (polarized) and *a-c* plane (depolarized), where the abscissa is the Raman shift. The spectra were excited at L_2 (t_{2g}) of Fig. 2. The SXES spectrum in the *a-b* plane corresponds to the spectrum *c* of Fig. 5(a). The large band at near −14eV is fluorescence, which accords with the Ti $3d$ PDOS in the valence band region. The intensity of Ti $3d$ PDOS is larger in the *a-c* plane. This result indicates that the hybridization between Ti $3d$ and O $2p$ is larger in the *a-c* plane.

Four Raman scattering peaks labeled as α, β, χ, and γ are observed in both *a-b* plane and *a-c* plane. The Raman shifts of α, β and χ in the *a-c* plane are smaller than those in the *a-b* plane. This behavior originates to the difference of lattice constant between *a-b* plane and *a-c* plane. The difference of lattice constant is reflected in the magnitude of crystal-field splitting (10Dq), which corresponds to the energy difference between t_{2g}- and e_g-subbands of Ti $3d$. Although the 10Dq in the *a-c* plane is not measured in this study, the magnitude is considered to be different from *a-b* plane. On the other hand, the intensity of Raman scattering peaks is larger in *a-c* plane. This corresponds to large hybridization effect between Ti $3d$ and O $2p$ state in the valence band.

4. CONCLUSION

We have studied the polarization dependence for the electronic structure of BIT single crystal using XAS and SXES. The valence band and conduction band are mainly composed of O $2p$ state and Ti $3d$ state, respectively. The SXES spectra measured at the Ti $2p$ absorption edge region exhibit three structures, which correspond to elastic scattering, fluorescence and soft-X-ray Raman scattering. The SXRS corresponds to the charge-transfer energy, which corresponds to the transition from O $2p$ state to Ti $3d$ state. The Raman shift of SXRS in the *a-c* plane is different from that in the *a-b* plane. The difference of CT energy originates to the lattice constant and hybridization effect in BIT single crystal.

ACKNOWLEDGEMENTS

We would like to Professor S. Shin of University of Tokyo for his useful discussion.

REFERENCES

[1] E. C. Subbarao: Phys. Rev. **122** (1961) 804.
[2] S. E. Cummins and L. E. Cross: Appl. Phys. Lett. **10** (1967) 14.
[3] R. W. Wolfe and R. E. Newnham: J. Electrochem. Soc. **116** (1967) 832.
[4] S. E. Cummins and L. E. Cross: J. Appl. Phys. **39** (1968) 2268.
[5] P. C. Joshi, A. Mansingh, M. N. Kamalasanen and S. Chandra: Appl. Phys. Lett. **59** (1991) 2389.
[6] W. Wu, K. Fumoto, Y. Oishi, M. Okuyama and Y. Hamakawa: Jpn. J. Appl. Phys. **35** (1996) 1560.
[7] H. Irie, H. Siito, S. Ohkoshi and K. Hashimoto: Adv. Meter. **17** (2005) 491.
[8] T. Takenaka and K. Sakata: Ferroelectrics **38** (1981) 769.
[9] Y. Noguchi, I. Miwa, Y. Goshima and M. Miyayama: Jpn. J. Appl. Phys. **39** (2000) L1259.
[10] T. Higuchi, M. Tanaka, K. Kudoh, T. Takeuchi, Y. Harada, S. Shin and T. Tsukamoto: Jpn. J. Appl. Phys. **40** (2001) 5803.
[11] M. Takahashi, Y. Noguchi and M. Miyayama: Jpn. J. Appl. Phys. **41** (2002) 7053.
[12] T. Higuchi, K. Kudoh, T. Takeuchi, Y. Masuda, Y. Harada, S. Shin and T. Tsukamoto: Jpn. J. Appl. Phys. **41** (2002) 7195.
[13] M. Soga, Y. Noguchi and M. Miyayama: Trans. Mater. Res. Soc. Jpn. **28** (2003) 173.
[14] M. Soga, Y. Noguchi, M. Miyayama, H. Okino and T. Yamamoto: Appl. Phys. Lett. **84** (2004) 100.
[15] T. Higuchi, Y. Noguchi, T. Goto, M. Miyayama, S. Shin, K. Kaneda, T. Hattori and T. Tsukamoto: Jpn. J. Appl. Phys. **44** (2005) L1491.
[16] T. Goto, Y. Noguchi, M. Soga and M. Miyayama: Mater. Res. Bull. **40** (2005) 1044.
[17] Y. Harada, T. Kinugasa, R. Eguchi, M. Matsubara, A. Kotani, M. Watanabe, A. Yagishita and S. Shin: Phys. Rev. B **61** (2000) 12854.
[18] S. Butorin, J. –H. Guo, M. Magnuson and J. Nordgren: Phys. Rev. B **55** (1997) 4242.
[19] Y. Tezuka, S. Shin, A. Agui, M. Fujisawa, and T. Ishii: J. Phys. Soc. Jpn, **65** (1996) 312.
[20] J. Jimenez-Mier, J. van Elk, D. L. Ederer, T. A. Callcott, J. J. Jia, J. Carlisle, L. Terminello, A. Asfaw, R. C. Perera, Phys. Rev. B **59** (1999) 2649.
[21] S. Shin, M. Fujisawa, H. Ishii, Y. Harada, M. Watanabe, M. M. Grush, T. A. Callcott, R. C. Perera, E. Z. Kurmaev, A. Moewes, R. Winarski, S. Stadler, D. L. Ederer, J. Electron Spectrosc. Relat. Phenom. **92** (1998) 197.
[22] S. M. Butorin, J. -H. Guo, M. Magnuson, P. Kuiper, and J. Nordgren, Phys. Rev. B **54** (1996) 4405.
[23] T. Higuchi, T. Tsukamoto, M. Watanabe, M. M. Grush, T. A. Callcott, R. C. Perera, D. L. Ederer, Y. Tokura, Y. Harada, Y. Tezuka and S. Shin: Phys. Rev. B **60** (1999) 7711.
[24] T. Higuchi, D. Baba, T. Takeuchi, T. Tsukamoto, Y. Taguchi, Y. Tokura, A. Chainani, and S. Shin: Phys. Rev. B **68** (2003) 104420-1.

(Received December 19, 2006;Accepted January 10, 2007)